





Capturing the stereoconfiguration of $(\text{C}_6\text{H}_6)_2\text{Ar}$ by Coulomb-explosion imaging

Xitao Yu , Yuqian Liu, Ke Deng, Xinyu Zhang, Pan Ma, Xiaokai Li , Chuncheng Wang , Zhonghua Cui,^{*}
Sizuo Luo ,[†] and Dajun Ding[‡]

*Institute of Atomic and Molecular Physics, Jilin University, Changchun 130012, People's Republic of China
and Jilin Provincial Key Laboratory of Applied Atomic and Molecular Spectroscopy, Jilin University,
Changchun 130012, People's Republic of China*



(Received 3 March 2022; accepted 24 May 2022; published 13 June 2022)

The configurations of the $(\text{C}_6\text{H}_6)_2\text{Ar}$ (Bz_2Ar) complex are identified by femtosecond laser-induced Coulomb explosion, in which the produced three-body coincident ionic momenta ($\text{Bz}^+ + \text{Bz}^+ + \text{Ar}^+$) is measured. The triangular structure is clearly determined by coincident momenta combined with quantum chemistry calculations, arising from classical trajectory simulations of eight promising configurations. Additionally, the bond distances between Ar and two Bz molecules are retrieved from the measured coincident momenta. The good agreement between measurement and computational calculations strongly suggests the laser-induced Coulomb explosion is a powerful approach for imaging configurations of the weakly bound molecular clusters.

DOI: [10.1103/PhysRevA.105.063105](https://doi.org/10.1103/PhysRevA.105.063105)

I. INTRODUCTION

Aromatic rings are known to be widespread in nature and play a vital role in physics, chemistry, and life sciences [1–3]. The interactions between aromatic molecules and other motifs, including π - π , π -H, and π -metal interactions, serve as significant contributions to the stability of DNA and proteins, drug binding, crystal engineering, and the formation of solid materials containing aromatic rings [4–7]. Molecular clusters consisting of benzene (C_6H_6 , Bz) are prototypical systems for studying these weak interactions, and they have been studied extensively by determining their structures. The stable configurations of the Bz dimer and trimer can be regarded to be a result of π - π interactions, which have captured extensive attention both experimentally and theoretically [5,8–11]. The molecular clusters formed by Bz molecules with other motifs also attracted great attention in the past few decades. The structures of Bz with rare gas (Rg), $\text{Bz-Rg}_{1,2}$ (Rg = He, Ne, Ar, Kr) have been measured by infrared spectra [12], and the complexes of Bz clusters bonded to the molecules H_2O , H_2S , OCS, and NO have been studied by measuring infrared and microwave spectra [13–17]. Besides those clusters containing π - π interactions with other motifs mentioned above, there is a set of emerging series consisting of two Bz molecules and one atom, which may involve the competition of π - π and π -atom interactions. The structures of Bz_2M ($M = \text{Sc-Zn}$) have been predicted theoretically and further determined by different methods [18–27], in which both the sandwich and triangular structures are involved and their configurations depend on the number of valence electrons of metal atoms. For $\text{Bz}_2\text{-Rg}$, valence orbitals of atoms are fully occupied, yet structures have still not been determined by either measurements or calculations.

Recently, the laser-induced Coulomb explosion (CE) was proven to be a great success in imaging structures of molecules and weakly bound complexes [28–37]. Kunitski *et al.* imaged the Efimov state of the helium trimer [38], Ren *et al.* observed the intermolecular Coulombic decay in Bz dimers [39], and Voigtsberger *et al.* disentangled the same trimer systems with different isotope atoms [40]. The structure of the H_2 dimer was determined via coincidence momentum imaging from femtosecond laser-induced CE, which proves hydrogen dimers are a mixture of all possible structural configurations [41]. Pickering *et al.* imaged structures of CS_2 and OCS dimers inside a He nanodroplet by combining the laser-induced alignment and CE [42,43]. Yu *et al.* determined the stereoconfiguration of OCS dimers based on a four-body coincidence measurement of fragments from laser-induced CE, where four isomers of the dimer are resolved and their structures are retrieved based on classical trajectory simulations [37]. This method has been demonstrated successfully on the simple molecular dimers mentioned above.

In the present work, the structure of Bz_2Ar is imaged from an intense femtosecond laser-pulse-induced CE, and the bond distances and angles between Ar and two Bz are retrieved via classical CE simulation (CCES). The structure of Bz_2Ar is further computed by quantum chemistry calculations and the isomerization energy decomposition analysis (IEDA). The measurement and computational calculations agree well, and both suggest the triangular structure is the most probable configuration of the Bz_2Ar complex.

II. EXPERIMENTAL AND COMPUTATIONAL METHODS

A. Experimental setup

The trimer, Bz_2Ar , formed by jet expansion of argon (1.2 bars) seeded with Bz into the vacuum through a nozzle with a diameter of 30 μm , is interacted with an 800-nm circularly polarized laser pulse (intensity of 6×10^{14} W/cm^2 , pulse duration of 40 fs, and repetition of 1 kHz) which is

^{*}zcui@jlu.edu.cn

[†]luosz@jlu.edu.cn

[‡]dajund@jlu.edu.cn

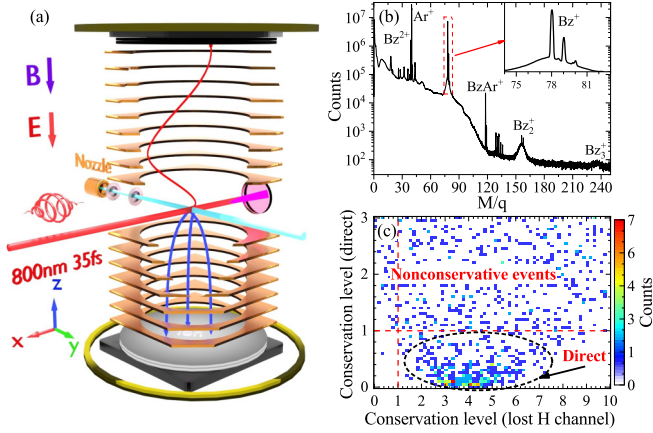


FIG. 1. (a) Schematic of the experimental setup. (b) The mass-to-charge spectrum of the total events. (c) The correlation map of the conservation level of the different channels.

focused by a concave mirror ($f = 7.5$ cm) in a cold-target recoil-ion-momentum spectrometer (COLTRIMS) [37,44,45], as shown in Fig. 1(a). Briefly, the produced ionic fragments are guided by a uniform electric field (19.8 V/cm) toward a time- and position-sensitive particle detector. Three-dimensional momenta of fragment ions are obtained from the measured position and time of flight (TOF) of signals. The typical measured TOF mass spectrum is shown in Fig 1(b). No obvious signal of Bz_2Ar^+ ions is observed, while previous research showed the Bz_2Ar^+ can be generated with quite low yield ratios relative to other clusters under similar conditions [46]. The circularly polarized laser is chosen to minimize the possible preferred selection of certain isomers during Coulomb-explosion imaging (CEI) due to the orientation-dependent ionization rate of molecule clusters in the laser-polarization direction [41]. The count rate is controlled to be less than 0.4 per pulse to keep the false coincidence rate sufficiently low.

The coincident events can be extracted by selecting three ionic fragments out of all detected particles according to a momentum-conservation condition. The momentum-conservation level δ for any three particles can be defined as

$$\delta = \frac{P_{\text{sum}_x}^2}{P_{\text{thre}_x}^2} + \frac{P_{\text{sum}_y}^2}{P_{\text{thre}_y}^2} + \frac{P_{\text{sum}_z}^2}{P_{\text{thre}_z}^2}, \quad (1)$$

where P_{sum_x} , P_{sum_y} , and P_{sum_z} are the components of the sum momentum of the three ions along the x , y , and z directions, respectively. p_{thre_x} , p_{thre_y} , and p_{thre_z} are 3 times the standard deviation of their corresponding distribution (13, 27, and 3.6 a.u. in our experiment, respectively). Events with $\delta < 1$ can be seen as meeting momentum conservation, and the smaller δ is, the better the conservation is.

To ensure the correctness of the channel selection, the condition $|P_{Bz^+/Ar^+}| > 20$ a.u. is applied to avoid false coincidences in which one or two fragments come from single ionization of the monomer. What is more, the possible existence of the hydrogen-loss reaction, $[Bz_2Ar]^{3+} \rightarrow C_6H_5^+ + Bz^+ + Ar^+ + H$, is distinguished from the direct channel, $[Bz_2Ar]^{3+} \rightarrow Bz^+ + Bz^+ + Ar^+$, by the correlation map of their conservation levels shown in Fig. 1(c). The correla-

tion map indicates that there is no hydrogen-loss event since the area which represents the hydrogen-loss channel shows a random distribution. The hydrogen-loss channel can also be excluded because no $C_6H_5^+$ signals from the Bz monomer in the mass spectrum are observed under the current experimental conditions, as shown in Fig. 1(b). The kinetic-energy release (KER) is calibrated by comparing the measured KER of $(Ar)_2$ from CE with previous measurements [34], and the uncertainty is estimated to be 0.1 eV.

B. Computation details

The geometrical optimization of Bz_2Ar is performed by density functional theory (DFT) using the Gaussian 09 software package, where the hybrid metageneralized gradient approximation exchange-correlation functionals M06-2X with 6-311G(d) basis set was used. The relative point groups and spectroscopic states are C_1 and 1A . During the optimization, over 30 structures are initially constructed by putting Ar atoms around stable benzene dimers, and only eight stable Bz_2Ar complexes are located as a local minimum with all positive vibrational frequencies.

The IEDA, which was successfully used to understand the structural preference of the isolated clusters [47–51], is performed within DFT using Perdew-Burke-Ernzerhof functional with dispersion (PBE-D) and the triple-zeta plus double polarization (TZ2P) basis set in ADF2020 package to determine the isomeric preference. This approach can be defined as follows:

$$\Delta E_{\text{iso}} = \Delta E_{\text{dist}}(Bz_2) + \Delta E_{\text{int}}, \quad (2)$$

where the energy difference between two isomers ΔE_{iso} is decomposed into two parts, including ΔE_{dist} and ΔE_{int} , where the former is the distortion energy of the respective constituents (two Bz_2 groups herein) in eight isomers relative to that of one isomer (isomer a here, as shown in Fig. 4 below). The interaction energy ΔE_{int} is the energy change when the prepared fragments are combined to form the complex. A quantitative energy decomposition analysis (EDA) divides the interaction energy into the electrostatic interaction ΔE_{elstat} , Pauli repulsion ΔE_{Pauli} , dispersion energy ΔE_{disp} , and attractive orbital interactions ΔE_{orb} :

$$\Delta E_{\text{int}} = \Delta E_{\text{elstat}} + \Delta E_{\text{Pauli}} + \Delta E_{\text{disp}} + \Delta E_{\text{orb}}, \quad (3)$$

where ΔE_{elstat} , which is usually attractive, is the energy between the unperturbed charge distributions of the prepared fragments. ΔE_{Pauli} is responsible for steric repulsion, which consists of the destabilizing interactions between occupied orbitals of the fragments. ΔE_{disp} constitutes the attractive part of the famous van der Waals (vdW) potentials. ΔE_{orb} accounts for charge transfer and polarization.

III. RESULTS AND DISCUSSION

Bz_2Ar dissociates after it is triply photoionized through a three-body CE channel, $[Bz_2Ar]^{3+} \rightarrow Bz^+ + Bz^+ + Ar^+$. To obtain the real events from the three-body CE channel, Fig. 2(a) shows the density plot of the momentum-conservation level δ of the three ions versus their total KER, which allows us to distinguish real coincidences from random ones [34,52]. Region a comes from the CE of the Bz_2Ar .

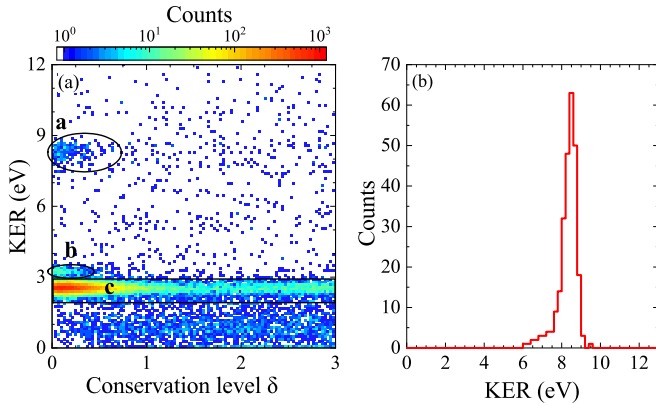


FIG. 2. (a) Density plot of the momentum-conservation level δ of the three ions versus their total KER. The δ value of coincident events is situated close to zero, and thus, real coincidences can be distinguished from random ones. The events in region a result from the CE of triply ionized Bz_2Ar . Region b comes from the CE of BzAr^{2+} and a singly ionized Bz molecule. Region c comes from CE of Bz_2^{2+} and a singly ionized Ar atom. (b) KER of $[\text{Bz}_2\text{Ar}]^{3+} \rightarrow \text{Bz}^+ + \text{Bz}^+ + \text{Ar}^+$ after applying momentum-conservation conditions.

Regions b and c come from false coincidences containing a singly ionized monomer and CE of BzAr or Bz_2 . Events from possible existing larger clusters Bz_nAr ($n > 2$), which should localize to the right of region a [34,52], can be neglected relative to the backgrounds. Other events come from false coincidences that could not be unambiguously identified. Combined with the momentum-conservation condition mentioned above, the real coincidences are selected, and the count is about 270. The corresponding KER of the selected events is shown in Fig. 2(b) with a single peak at 8.4 eV.

The dissociation dynamics of the three-body CE of Bz_2Ar should be determined first before imaging the structure since three-body fragmentation can occur through both sequential and concerted processes [30,53]; particularly, a sequential fragmentation process will provide misleading information about the accuracy and the reliability of structural reconstruction for molecular clusters [54]. Generally, a sequential fragmentation channel will show energy correlations among fragments, which provides a clue to identifying the sequential process [37,55]. Figure 3(a) gives the correlation map of the kinetic energy of the three ions in a Dalitz plot [56], which shows their energy correlations in a triangular coordinate system and the coordinates can be expressed as

$$X = (E_1 - E_2)/(\sqrt{3}W), \quad Y = E_3/W - 1/3. \quad (4)$$

where E_1 , E_2 , and E_3 are the kinetic energies of fragments and $W = E_1 + E_2 + E_3$. This kind of Dalitz plot related to energy is usually elliptical because the momentum-conservation condition under the energy representation is related to the mass of fragments, which is different in most cases [56,57]. The distribution of the Dalitz plot in Fig. 3(a) mainly contributes near the coordinate (0, 0.12), indicating that the kinetic energies of the fragments have a fixed correlation and the fragments are generated simultaneously. In another perspective, the signal from sequential fragmentation events always presents as linear distributions [30,54] because the kinetic energy of the

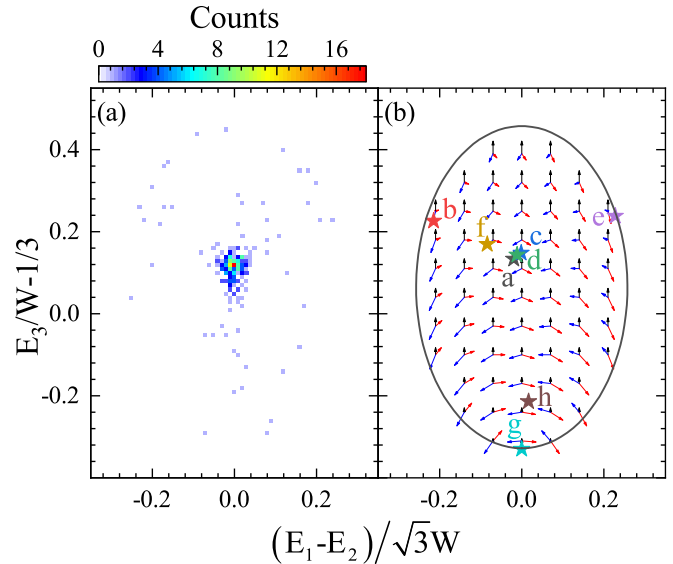


FIG. 3. (a) Dalitz plot of the events from three-body CE of Bz_2Ar , where E_1 and E_2 correspond to the kinetic energy of Bz^+ and E_3 corresponds to that of Ar^+ . The distribution is centered at (0, 0.12). (b) Simulated positions of calculated isomers in the Dalitz plot; the relative momentum vectors of the three ions are shown as arrows, red and blue for Bz and black for Ar.

fragment generated in the first step is irrelevant to the other fragments. The distribution indicates that only a concerted fragmentation process occurs during the three-body CE of the Bz_2Ar , which may be attributed to the weak vdW interactions between the monomer molecules and atoms. Thus, we can use all these measured events to further deduce their structure.

The structure of Bz_2Ar can be preliminarily determined by the relative momenta of the three ions by simulating the mapping between the momentum and structure. Figure 3(b) gives the corresponding momentum vectors of the three ions for various coordinates in the Dalitz plot. The measured result at coordinate (0, 0.12) corresponds to a momentum composition of the angle between the momenta of two Bz^+ of about 125° and the angle between the momenta of Bz^+ and Ar^+ of about 117° . This momentum configuration can retrieve two potential candidate structures, $(56^\circ, 62^\circ, 62^\circ)$ and $(120^\circ, 30^\circ, 30^\circ)$ in the angle order of $(\angle\text{Bz-Ar-Bz}, \angle\text{Ar-Bz-Bz}, \angle\text{Ar-Bz-Bz})$, by a point-charge-approximated CE simulation since the mapping between the momentum and structure is nonunique [58].

However, it is not enough to determine which structure is the real one using the current information, and further quantum chemical computations are necessary to distinguish the two geometries. The optimized structures of the eight isomers of Bz_2Ar are shown in Fig. 4, showing mainly two types of isomers, triangularly distributed structures (isomers a, c, d, and f) and nearly linearly distributed structures (isomers b, e, g, and h). The distances and relative angles among the center-of-mass (c.m.) of the constituents of Bz_2Ar are given in Table I. The results show that the geometries of isomers a, c, and d are close to the structure $(56^\circ, 62^\circ, 62^\circ)$, and no isomer corresponds to the other preliminary candidate. This means that the structure of Bz_2Ar is likely to be like isomers a, c, and d with nearly equilateral triangular structures.

TABLE I. Distance and relative angle among the c.m. of the constituents of Bz_2Ar and their relative energy computed at the M062x/6-311G(d) levels with zero-point corrections of M062x/6-311G(d) for various isomers. The Coulomb potentials between constituents after threefold ionization are included.

	Isomer							
	a	b	c	d	e	f	g	h
R_{BzBz} (Å)	4.6	3.8	3.8	3.9	4.8	4.9	6.8	8.3
R_{BzAr} (Å)	4.4	6.9	4.6	4.5	3.3	8.4	3.4	5
R_{BzAr} (Å)	3.3	3.3	4.6	5	8.1	4.8	3.4	3.3
$\angle Bz-Ar-Bz$ (deg)	71.5	14.7	49.3	48.8	7.2	30	177.7	168.7
$\angle Ar-Bz-Bz$ (deg)	65.9	12.6	65.3	72.9	167.8	120.9	1.1	6.8
$\angle Ar-Bz-Bz$ (deg)	42.6	152.7	65.3	58.2	5	29.1	1.2	4.5
Energy (kcal/mol)	0	0.3	0.3	0.6	0.7	1.8	2.8	3.4
Coulomb potential (eV)	9.4	8.2	9.4	9.1	7.8	7.5	8.5	8.0

Moreover, we also simulate the position of the Dalitz plot for these isomers based on the CCES of the three-body CE of Bz_2Ar . In the simulation, the rotation of the two Bz^+ is ignored, and the averaged Mulliken charge distribution of Bz^+ ($\delta_H = 0.212$, $\delta_C = -0.046$) has been used in calculating the Coulomb force among fragments. The Newton equations of the ions can be expressed as

$$\sum_{j=1, j \neq i}^3 \sum_{k,m=1}^N \frac{q_{ik}q_{jm}}{|r_{ik,jm}|^3} \vec{r}_{ik,jm} = m_i \ddot{\vec{r}}_{ic}, \quad (5)$$

where \vec{r}_{ik} and q_{ik} represent the position vector and charge of the k th partial charge of the i th fragments, respectively, $\vec{r}_{ik,jm}$ represents the vector pointing from \vec{r}_{ik} to \vec{r}_{jm} , and $\ddot{\vec{r}}_{ic}$ is the second derivative of the c.m. position vector of the i th ions. The simulated position shown in Fig. 3(b) also indicates that the structure of Bz_2Ar is likely to be like isomers a, c, and d since the positions of isomers a, c, and d are close to the measured one, while those of the other five isomers, isomers b, e, f, g, and h, are away from the measured results.

The reason why only the triangular structure is confirmed experimentally may be attributed to their generally lower energies compared with those of linearly distributed isomers

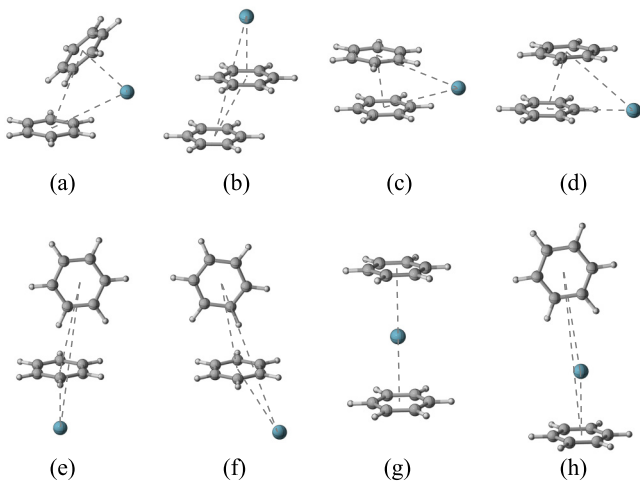


FIG. 4. The optimized structures of low-lying energy isomers of Bz_2Ar determined by M06-2X/6-311G(d).

which may have more population, as shown in Table I. However, no signal corresponds to isomer b in the Dalitz plot, even though isomer b may have populations similar to those of isomers c and d because of their close total energy. To further understand such a structure preference, we have performed an IEDA, and the results are given in Table II, where the values of ΔE_{iso} from the IEDA formula are consistent with the relative energy trend given in Table I. The sum of two terms, ΔE_{dist} (Bz_2) and ΔE_{int} , determines the isomeric preference. Isomers a, b, and c have the same ΔE_{dist} (Bz_2) values, while isomer a has lower ΔE_{int} compared to the other two, which indicates the interaction energy dominates the contribution of cluster stabilization. The significant ΔE_{dist} (Bz_2) affects the thermodynamic stability of isomers d, e, and f compared to isomer a, although they have considerable ΔE_{int} . Isomers g and h possess weak structural preference because ΔE_{dist} (Bz_2) and ΔE_{int} are both unfavorable. In the lowest-energy isomer, isomer a, the considerable ΔE_{elstat} and ΔE_{disp} provide a driving force to stabilize such intriguing complexes.

The structure of Bz_2Ar can be reconstructed in coordinate space by fitting the simulated momenta to the measured ones for various initial structures using a genetic algorithm. The number of probable reconstructed structural parameters is only three for a three-body CE coincidence measurement because three degrees of freedom from the constraint of momentum conservation and three degrees of freedom from the random orientation of the trimer should be subtracted from the nine total dimensions of momenta of the three fragments.

TABLE II. The IEDA results of the Bz_2Ar cluster (in kcal/mol), considering one Ar atom with two neutral Bz groups as interacting fragments at the PBE-D/TZ2P-ZORA level.

Energy	Isomer							
	a	b	c	d	e	f	g	h
ΔE_{iso}	-4.4	-3.6	-3.8	-3.5	-2.4	-1.8	-1.8	-1.7
ΔE_{dist}	0	0	0	0.5	1.8	2	0.4	0.4
ΔE_{int}	-4.4	-3.6	-3.8	-4	-4.2	-3.8	-2.2	-2.1
ΔE_{Pauli}	7.6	7.4	7.8	4.9	5.7	3.1	3.2	2.2
ΔE_{elstat}	-4.3	-3.6	-3.7	-2.5	-3.4	-2.2	-1.7	-1.4
ΔE_{disp}	-5.6	-5.6	-5.9	-4.9	-4.6	-3.3	-2.9	-2.2
ΔE_{orb}	-2.1	-1.8	-2.2	-1.5	-1.8	-1.4	-0.7	-0.7

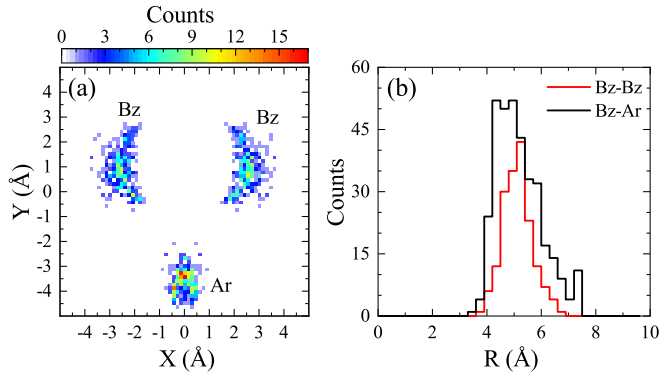


FIG. 5. (a) The reconstructed spatial distribution of three monomers. Coordinates are rotated to the molecular frame of reference, where the c.m. of the trimer defines the origin and the angular bisector of the angle Bz-Ar-Bz defines the y axis. All other coordinates are oriented relative to these definitions. (b) The distribution of intermolecular distances of Bz-Bz and Bz-Ar in coordinate space.

Only the structure of their c.m. can be reconstructed, and the orientation of the Bz cannot be obtained. During the reconstruction, the relative orientations of the two Bz^+ are set to be the same as that of isomer a since isomer a is the most probable from the calculation. All bond angles are limited to less than 90° during the reconstruction since all the bond angles are acute angles for isomer a. The goodness parameter η can be given as

$$\eta = \sum_{i=1}^N |p_i^e - p_i^s|, \quad (6)$$

where p_i^e and p_i^s are the magnitudes of the momentum of the i th ion from experiment and simulation, respectively.

The reconstructed structure of the c.m. of two Bz molecules and Ar is given in Fig. 5(a), with their corresponding bond lengths shown in Fig. 5(b). The distribution indicates that the most probable structure of Bz_2Ar is a nearly regular triangle. The most probable value of R_{BzBz} from the experimental reconstruction is about $5.0 \pm 0.4 \text{ \AA}$, and that of R_{BzAr} is about $4.7 \pm 0.8 \text{ \AA}$, a little larger than that from the calculated structure in Table I. Such overestimation of intermolecular distance is also reflected in the difference between the KER and the Coulomb potential among constituents which is given in Table I, where the Coulomb potential energies of the triangle isomers a (9.4 eV), c (9.4 eV), and d (9.1 eV) are higher than the measured KER peak at 8.4 eV. The lower KER relative to the Coulomb potential may originate from the non-Coulomb effects [36], polarization between fragments which may enlarge the distance between the charges relative

to the geometrical distance, and the undetected internal energy during the dissociation, such as the vibrational and rotational energies of the Bz. The longer distance of Bz-Ar relative to the calculation may also result from faster vibration of the Ar atom than the Bz molecule due to the lower weight of the Ar atom relative to the Bz molecule.

The clusters of Bz_2M ($M=\text{Sc-Zn}$) mainly have sandwich structures ($M=\text{Sc-Ni}$) and triangular structures ($M=\text{Cu, Zn}$), as has been reported from experiments and calculations [18–27]. However, the most probable structure of Bz_2Ar has a triangular structure, as indicated by both the measurement and quantum chemical calculation in our work, which is similar to the configuration of Bz_2Cu and Bz_2Zn . The formation of the triangular structures of Bz_2M ($M=\text{Cu, Zn}$) was ascribed to the very weak interaction between Cu (Zn) and Bz relative to the π -H interaction between two benzene molecules [21] due to their fully occupied valence orbitals of atoms. And the structure is no longer a stacked form. Similarly, for the Bz_2Ar system, the valence orbitals of Ar are also fully occupied, the interaction between Ar and Bz is very weak, and the π -H interaction is dominant, leading to triangular structures.

IV. CONCLUSION

The configurations of the $(\text{Bz})_2\text{Ar}$ complex were imaged by using laser-induced CE and predicted from quantum chemistry calculations. Experimentally, the momenta of three fragment ions from CE of $[\text{Bz}_2\text{Ar}]^{3+} \rightarrow \text{Bz}^+ + \text{Bz}^+ + \text{Ar}^+$ were coincidentally measured with the COLTRIMS, and the structures with triangle distributions were confirmed by the CCES combined with quantum calculations. Theoretically, there are eight local minimums predicted by the M062x/6-311G(d) level, and the most stable structure has a triangle distribution. Note that this structure agrees quite well with our measurement. Furthermore, the structural parameters between Ar and two Bz molecules were retrieved from the measured coincident momenta by comparing the measured momenta with those simulated from CCES for various initial structures using a genetic algorithm. The agreement between experimental and theoretical results indicates that the unknown configurations of the molecular clusters can be imaged by femtosecond laser-induced CE.

ACKNOWLEDGMENTS

This work was supported by the National Basic Research Program of China (Grant No. 2019YFA0307701), by the National Natural Science Foundation of China (Grants No. 12074143, No. 12134005, No. 11627807, No. 11922405, and No. 11904120), and by the Fundamental Research Funds for the Central Universities.

- [1] L. M. Salonen, M. Ellermann, and F. Diederich, *Angew. Chem., Int. Ed.* **50**, 4808 (2011).
 [2] E. C. Lee, D. Kim, P. Jurečka, P. Tarakeshwar, P. Hobza, and K. S. Kim, *J. Phys. Chem. A* **111**, 3446 (2007).
 [3] S. E. Wheeler and J. W. G. Bloom, *J. Phys. Chem. A* **118**, 6133 (2014).

- [4] C. A. Hunter and J. K. M. Sanders, *J. Am. Chem. Soc.* **112**, 5525 (1990).
 [5] M. O. Sinnokrot, E. F. Valeev, and C. D. Sherrill, *J. Am. Chem. Soc.* **124**, 10887 (2002).
 [6] S. Burley and G. Petsko, *Science* **229**, 23 (1985).
 [7] H. F. Noller, *Science* **309**, 1508 (2005).

- [8] M. Schnell, U. Erlekam, P. R. Bunker, G. von Helden, J.-U. Grabow, G. Meijer, and A. van der Avoird, *Angew. Chem., Int. Ed.* **52**, 5180 (2013).
- [9] M. O. Sinnokrot and C. D. Sherrill, *J. Phys. Chem. A* **110**, 10656 (2006).
- [10] P. C. Jha, Z. Rinkevicius, H. Ågren, P. Seal, and S. Chakrabarti, *Phys. Chem. Chem. Phys.* **10**, 2715 (2008).
- [11] M. Pitoňák, P. Neogrady, J. Řezáč, P. Jurečka, M. Urban, and P. Hobza, *J. Chem. Theory Comput.* **4**, 1829 (2008).
- [12] K. Esteki, A. J. Barclay, A. R. W. McKellar, and N. Moazzen-Ahmadi, *Chem. Phys. Lett.* **713**, 65 (2018).
- [13] R. N. Pribble and T. S. Zwier, *Science* **265**, 75 (1994).
- [14] B. Chiavarino, M. E. Crestoni, S. Fornarini, J. Lemaire, P. Maître, and L. MacAleese, *J. Am. Chem. Soc.* **128**, 12553 (2006).
- [15] M. Dehghany, J. Norooz Oliace, M. Afshari, N. Moazzen-Ahmadi, and A. R. W. McKellar, *J. Chem. Phys.* **132**, 194303 (2010).
- [16] Y. Zeng, J. Hao, S. Zheng, and L. Meng, *J. Phys. Chem. A* **115**, 11057 (2011).
- [17] E. Arunan, T. Emilsson, and H. S. Gutowsky, *J. Chem. Phys.* **101**, 861 (1994).
- [18] B. R. Sohnlein, Y. Lei, and D.-S. Yang, *J. Chem. Phys.* **127**, 114302 (2007).
- [19] B. R. Sohnlein, S. Li, and D.-S. Yang, *J. Chem. Phys.* **123**, 214306 (2005).
- [20] R. Pandey, B. K. Rao, P. Jena, and M. A. Blanco, *J. Am. Chem. Soc.* **123**, 3799 (2001).
- [21] I. S. Youn, D. Y. Kim, N. J. Singh, S. W. Park, J. Youn, and K. S. Kim, *J. Chem. Theory Comput.* **8**, 99 (2012).
- [22] D. Rayane, A.-R. Allouche, R. Antoine, M. Broyer, I. Compagnon, and P. Dugourd, *Chem. Phys. Lett.* **375**, 506 (2003).
- [23] A. K. Kandalam, B. K. Rao, P. Jena, and R. Pandey, *J. Chem. Phys.* **120**, 10414 (2004).
- [24] K. Hoshino, T. Kurikawa, H. Takeda, A. Nakajima, and K. Kaya, *J. Phys. Chem.* **99**, 3053 (1995).
- [25] K. Miyajima, S. Yabushita, M. B. Knickelbein, and A. Nakajima, *J. Am. Chem. Soc.* **129**, 8473 (2007).
- [26] N. Zhang, H. Du, J. Chang, W. Jin, C. Li, G. Lefkidis, and W. Hübner, *Phys. Rev. B* **98**, 104431 (2018).
- [27] X. Zhang and J. Wang, *J. Phys. Chem. A* **112**, 296 (2008).
- [28] Z. Vager, R. Naaman, and E. P. Kanter, *Science* **244**, 426 (1989).
- [29] Y. Muramatsu, K. Ueda, N. Saito, H. Chiba, M. Lavollée, A. Czasch, T. Weber, O. Jagutzki, H. Schmidt-Böcking, R. Moshhammer, U. Becker, K. Kubozuka, and I. Koyano, *Phys. Rev. Lett.* **88**, 133002 (2002).
- [30] N. Neumann, D. Hant, L. P. H. Schmidt, J. Titze, T. Jahnke, A. Czasch, M. S. Schöffler, K. Kreidi, O. Jagutzki, H. Schmidt-Böcking, and R. Dörner, *Phys. Rev. Lett.* **104**, 103201 (2010).
- [31] M. Pitzer, M. Kunitski, A. S. Johnson, T. Jahnke, H. Sann, F. Sturm, L. P. H. Schmidt, H. Schmidt-Böcking, R. Dörner, J. Stohner, J. Kiedrowski, M. Reggelin, S. Marquardt, A. Schießer, R. Berger, and M. S. Schöffler, *Science* **341**, 1096 (2013).
- [32] P. Herwig, K. Zawatzky, M. Grieser, O. Heber, B. Jordon-Thaden, C. Krantz, O. Novotny, R. Repnow, V. Schurig, D. Schwalm, Z. Vager, A. Wolf, O. Trapp, and H. Kreckel, *Science* **342**, 1084 (2013).
- [33] U. Ablikim, C. Bomme, H. Xiong, E. Savelyev, R. Obaid, B. Kaderiya, S. Augustin, K. Schnorr, I. Dumitriu, T. Osipov, R. Bilodeau, D. Kilcoyne, V. Kumarappan, A. Rudenko, N. Berrah, and D. Rolles, *Sci. Rep.* **6**, 38202 (2016).
- [34] B. Ulrich, A. Vredenburg, A. Malakzadeh, L. P. H. Schmidt, T. Havermeier, M. Meckel, K. Cole, M. Smolarski, Z. Chang, T. Jahnke, and R. Dörner, *J. Phys. Chem. A* **115**, 6936 (2011).
- [35] J. Wu, M. Kunitski, L. P. H. Schmidt, T. Jahnke, and R. Dörner, *J. Chem. Phys.* **137**, 104308 (2012).
- [36] C. A. Schouder, A. S. Chatterley, L. B. Madsen, F. Jensen, and H. Stapelfeldt, *Phys. Rev. A* **102**, 063125 (2020).
- [37] X. Yu, X. Zhao, Z. Wang, Y. Yang, X. Zhang, P. Ma, X. Li, C. Wang, X. Xu, C. Wang, D. Zhang, S. Luo, and D. Ding, *Phys. Rev. A* **104**, 053104 (2021).
- [38] M. Kunitski, S. Zeller, J. Voigtsberger, A. Kalinin, L. P. H. Schmidt, M. Schöffler, A. Czasch, W. Schöllkopf, R. E. Grisenti, T. Jahnke, D. Blume, and R. Dörner, *Science* **348**, 551 (2015).
- [39] X. Ren, J. Zhou, E. Wang, T. Yang, Z. Xu, N. Sisourat, T. Pfeifer, and A. Dorn, *Nat. Chem.* **14**, 232 (2022).
- [40] J. Voigtsberger, S. Zeller, J. Becht, N. Neumann, F. Sturm, H.-K. Kim, M. Waitz, F. Trinter, M. Kunitski, A. Kalinin, J. Wu, W. Schöllkopf, D. Bressanini, A. Czasch, J. B. Williams, K. Ullmann-Pfleger, L. P. H. Schmidt, M. S. Schöffler, R. E. Grisenti, T. Jahnke, and R. Dörner, *Nat. Commun.* **5**, 5765 (2014).
- [41] A. Khan, T. Jahnke, S. Zeller, F. Trinter, M. Schöffler, L. P. H. Schmidt, R. Dörner, and M. Kunitski, *J. Phys. Chem. Lett.* **11**, 2457 (2020).
- [42] J. D. Pickering, B. Shepperson, B. A. K. Hübschmann, F. Thorning, and H. Stapelfeldt, *Phys. Rev. Lett.* **120**, 113202 (2018).
- [43] J. D. Pickering, B. Shepperson, L. Christiansen, and H. Stapelfeldt, *J. Chem. Phys.* **149**, 154306 (2018).
- [44] J. Ullrich, R. Moshhammer, A. Dorn, R. Dörner, L. P. H. Schmidt, and H. Schmidt-Böcking, *Rep. Prog. Phys.* **66**, 1463 (2003).
- [45] S. Luo, J. Liu, X. Li, D. Zhang, X. Yu, D. Ren, M. Li, Y. Yang, Z. Wang, P. Ma, C. Wang, J. Zhao, Z. Zhao, and D. Ding, *Phys. Rev. Lett.* **126**, 103202 (2021).
- [46] B.-M. Cheng, E. A. Walters, and J. R. Grover, *AIP Adv.* **9**, 125005 (2019).
- [47] M. Contreras, E. Osorio, F. Ferraro, G. Puga, K. J. Donald, J. G. Harrison, G. Merino, and W. Tiznado, *Chem. Eur. J.* **19**, 2305 (2013).
- [48] A. Vásquez-Espinal, K. Palacio-Rodríguez, E. Ravell, M. Orozco-Ic, J. Barroso, S. Pan, W. Tiznado, and G. Merino, *Chem. - Asian J.* **13**, 1751 (2018).
- [49] E. Ravell, S. Jalife, J. Barroso, M. Orozco-Ic, G. Hernández-Juárez, F. Ortiz-Chi, S. Pan, J. L. Cabellos, and G. Merino, *Chem. - Asian J.* **13**, 1467 (2018).
- [50] D. Moreno, G. Martínez-Guajardo, A. Díaz-Celaya, J. M. Mercero, R. de Coss, N. Perez-Peralta, and G. Merino, *Chem. - Eur. J.* **19**, 12668 (2013).
- [51] A. C. Castro, E. Osorio, J. L. Cabellos, E. Cerpa, E. Matito, M. Solà, M. Swart, and G. Merino, *Chem. - Eur. J.* **20**, 4583 (2014).
- [52] B. Ulrich, A. Vredenburg, A. Malakzadeh, M. Meckel, K. Cole, M. Smolarski, Z. Chang, T. Jahnke, and R. Dörner, *Phys. Rev. A* **82**, 013412 (2010).

- [53] C. Wu, C. Wu, D. Song, H. Su, Y. Yang, Z. Wu, X. Liu, H. Liu, M. Li, Y. Deng, Y. Liu, L.-Y. Peng, H. Jiang, and Q. Gong, *Phys. Rev. Lett.* **110**, 103601 (2013).
- [54] X. Q. Hu, Y. G. Peng, X. L. Zhu, S. C. Yan, L. Liu, W. T. Feng, D. L. Guo, Y. Gao, S. F. Zhang, D. M. Zhao, D. P. Dong, B. Hai, J. W. Xu, S. B. Zhang, X. Ma, J. G. Wang, and Y. Wu, *Phys. Rev. A* **101**, 012707 (2020).
- [55] X. Zhao, T. Xu, X. Yu, D. Ren, X. Zhang, X. Li, P. Ma, C. Wang, D. Zhang, Q. Wang, X. Hu, S. Luo, Y. Wu, J. Wang, and D. Ding, *Phys. Rev. A* **103**, 053103 (2021).
- [56] R. Dalitz, *London, Edinburgh, Dublin Philos. Mag. J. Sci.* **44**, 1068 (1953).
- [57] B. Wales, É. Bisson, R. Karimi, S. Beaulieu, A. Ramadhan, M. Giguère, Z. Long, W.-K. Liu, J.-C. Kieffer, F. Légaré, and J. Sanderson, *J. Electron Spectrosc. Relat. Phenom.* **195**, 332 (2014).
- [58] A. M. Sayler, E. Eckner, J. McKenna, B. D. Esry, K. D. Carnes, I. Ben-Itzhak, and G. G. Paulus, *Phys. Rev. A* **97**, 033412 (2018).